Optical Engineering

SPIEDigitalLibrary.org/oe

Effect of working gas pressure on interlayer mixing in magnetron-deposited Mo/Si multilayers

Yuriy P. Pershyn
Eric M. Gullikson
Valeriy V. Kondratenko
Valentine V. Mamon
Svetlana A. Reutskaya
Dmitriy L. Voronov
Evgeniy N. Zubarev
Igor A. Artyukov
Alexander Vladimirovich Vinogradov

Effect of working gas pressure on interlayer mixing in magnetron-deposited Mo/Si multilayers

Yuriy P. Pershyn
National Technical University
Kharkiv Polytechnic Institute
Metal and Semiconductor Physics Department
Frunze Street 21
Kharkiv 61002, Ukraine
E-mail: persh@kpi.kharkov.ua

Eric M. Gullikson
Lawrence Berkeley National Laboratory
Berkeley, California 94720

Valeriy V. Kondratenko
Valentine V. Mamon
Svetlana A. Reutskaya
National Technical University
Kharkiv Polytechnic Institute
Metal and Semiconductor Physics Department
Frunze Street 21
Kharkiv 61002, Ukraine

Dmitriy L. Voronov
Lawrence Berkeley National Laboratory
Berkeley, California 94720

Evgeniy N. Zubarev
National Technical University
Kharkiv Polytechnic Institute
Metal and Semiconductor Physics Department
Frunze Street 21
Kharkiv 61002, Ukraine

Igor A. Artyukov
Alexander Vladimirovich Vinogradov
P.N. Lebedev Physical Institute
Moscow 117942, Russia

Abstract. By methods of cross-sectional transmission electron microscopy and small-angle x-ray scattering ($\lambda = 0.154$ nm) the influence of Ar gas pressure (1 to 4 mTorr) on the growth of amorphous interfaces in Mo/Si multilayers (MLs) deposited by DC magnetron sputtering is studied. The significant reduction in the ML period, which is evident as a volumetric contraction, is observed in MLs deposited at Ar pressure where the mean-free path for the sputtered atoms is comparable with the magnetron-substrate distance. Some reduction in the thickness of the amorphous interlayers with Ar pressure increase is found, where the composition of the interlayers is enriched with molybdenum. The interface modification resulted in an increase in EUV reflectance of the Mo/Si MLs. [DOI: 10.1117/1.OE.52.9.095104]

Subject terms: x-ray multilayer mirrors; interfaces; composition; Ar pressure influence; silicides.

Paper 130648P received Apr. 30, 2013; revised manuscript received Aug. 19, 2013; accepted for publication Aug. 20, 2013; published online Sep. 20, 2013.

1 Introduction

The performance of an x-ray optical instrument is defined by both the efficiency of the optical scheme and characteristics of the optical components included. Multilayer x-ray mirrors (MXMs) are optical elements designed to provide reflectance within the range of soft x-rays and extreme ultraviolet (1 to 100 nm), especially close to normal incidence angles.[1–5] The fabrication of MXMs has advanced to the point where for a particular MXM, the limiting characteristics are substantially defined by the state of the interfaces, namely, the roughness and the level of layer intermixing. Rough interfaces scatter radiation in the nonspecular direction, and intermixed or diffuse interlayers decrease the gradient of optical constants (refractive indices); these factors lower the reflection amplitude at each interface, raising the effective absorption, and finally, decreasing the MXM efficiency. Utilization of modern techniques of film deposition (both evaporation and sputtering) provides a good reproducibility of surface relief and together with the availability of smooth substrates (roughness $\sigma \leq 0.2$ nm), this reduces to a considerable extent the problem of roughness at the interfaces. However, roughness is still an issue to the region of short-period multilayers (MLs) (periods $d < 2$–2.5 nm).

MXMs based on the material pair of Mo and Si have a variety of applications within the wavelength range of 12.3 to 25.0 nm. They have been subjected to intense study as a promising candidate for projective x-ray lithography at the wavelength of ~13.6 nm.[6–9] Mo/Si MXMs lent impetus to the development of x-ray microscopes,[10,11] telescopes,[12,13] spectroscopes,[14,15] and interferometers.[16–18] They also found specific applications such as polarizers,[19–21] phase shifters,[22–24] beam splitters,[25–27] and broadband mirrors.[28–30]

Both Mo-on-Si and Si-on-Mo interfaces in MXMs have intermixed interlayers since according to the phase diagram[31]

0091-3286/2013/$25.00 © 2013 SPIE

Mo and Si can form chemical compounds. Interlayers are amorphous[32] and have a silicide nature; their width varies over a wide range [from ~0.5 (Ref. 33) up to ~4 (Ref. 34) nm]. The degree of intermixing is usually associated with the energy of deposited atoms typical of a particular deposition method. The most intermixing is observed in MXMs deposited by diode,[35] triode, or ion-beam[34,36] sputtering. The least intermixing is common in the case of magnetron sputtering[36–38] and e-beam evaporation combined with the ion-beam polishing.[39–41] In addition, the interlayer thickness at Si-on-Mo interface was found to depend on the structural state of the Mo layer: in amorphous molybdenum, it is twice as large as in crystalline Mo.[38,42,43] The mechanism of the interface formation is not fully understood and is the subject of wide speculation, particularly, with regard to asymmetric interfaces.[32,33,44–46] Several models explaining the asymmetry in interface formation have been suggested.[34,37,42,47,48]

Most researchers suggest that the amorphous interlayers at Mo/Si interfaces have a composition close to $MoSi_2$.[35,38,43,47,49–53] The formation of this silicide is in agreement with the Bene–Walser rule on the first phase nucleating at the interfaces.[54] However, some authors present results on the existing of lower silicides (Mo_5Si_3 or Mo_3Si) rather than the disilicide.[39,55]

For the usual wavelength range of applications, the period of Mo/Si MXMs should exceed 6 nm. Thus with a typical interface roughness of $\sigma \sim 0.3$ to 0.4 nm, the influence of roughness on their optical characteristics will be minor. With the range of intermixing given above, interlayers should be the main defect of Mo/Si MXMs.

A number of studies focused on improving the reflectivity of Mo/Si MLs by the control of the interface state through a change in the energy of deposited atoms.[56–58] The sputtering gas pressure has also been shown to influence the interface roughness[49,59,60] and mechanical stress.[61,62] In this work, we demonstrate that a variation in the working gas pressure affects the width and the composition of the amorphous interlayers. The detailed information on the composition and the width of interlayers will allow for proper optimization of the optical characteristics of a particular Mo/Si MXM.

2 Experimental Methods

The ML mirrors were fabricated by DC magnetron sputtering while the discharge currents of the Si and Mo magnetrons as well as the Ar pressure were held constant to provide a stable deposition rates. A series of mirrors were fabricated under different pressure conditions with the deposition rates for molybdenum and silicon of 0.35 to 0.42 and 0.45 to 0.65 nm/s, respectively. The ML periods were estimated to be in the range of 6 to 9 nm.

All the MXMs were deposited onto polished silicon wafers and float glass with a root mean square surface roughness of 0.3 to 0.5 nm. The purity of the 100-mm diameter magnetron targets was 99.5% and 99.99% for Mo and Si, respectively. The distance between the magnetron surface and the deposited substrate was about 30 mm.

ML structures were studied using a small-angle x-ray diffractometer, the DRON-3M [two-crystal spectrometer scheme with a single crystal Si (110) monochromator]. A 0.1-mm slit after the monochromator provided selection of the Cu $K\alpha_1$ line from an x-ray tube with a copper anode. Periodicity for each ML stack was defined with the full Bragg equation (taking into account refraction). Errors in period measurements were <0.01 nm. The phase analysis was carried out at the same wavelength with the help of another diffractometer equipped with a graphite analyzer.

The effect of the plasma above the magnetron target on the growing films was investigated by measuring the potential induced at the substrate with a Langmuir probe consisting of tungsten wire 0.2-mm thick located within a ceramic tube.

We estimated the relative content of molybdenum in ML samples by x-ray fluorescence analysis using an x-ray crystal-diffraction spectrometer, SPRUT (Ukrrentgen, Ukraine).

Cross-sections of Mo/Si MXMs were studied with a transmission electron microscope (TEM) (PEM-U) with an accelerating voltage of 100 kV. The electron microscopy resolution measured by lines (atomic planes) is 0.2 nm.

EUV measurements of MXM reflectivity were performed at beamline 6.3.2 of the advanced light source.[63,64] Briefly, the beamline contains a four-jaw aperture, three grazing incident mirrors working in the total external reflection region, the monochromator including three variable space (graded period) gratings, exit slit, order suppressor, and a detector. The design provides a high spectral purity, relative spectral bandwidth $\lambda/\Delta\lambda \leq 700$ and high precision of reflectivity measurement ($\Delta R/R \approx 0.2\%$) with a beam size of $10 \times 300\ \mu m^2$.

3 Results

3.1 *Preliminary Procedures*

Ballistic mixing is considered as one of the probable mechanisms for interlayer formation for sputter-deposited MLs;[48] we have tried to reduce this effect by decreasing the energy of particles impinging on a growing surface. To do this, we varied the gas pressure inside the vacuum chamber. When the mean-free path for sputtered atoms becomes comparable to the distance from the magnetron to the substrate, the energy of the atoms decreases, and further increase of the pressure must eventually thermalize the sputtered atoms.

Figure 1 shows a schematic view of a magnetron unit used for layer deposition. The substrate is fixed on a rotating substrate holder and major time covered by Mo (Si) in a position denoted by numeral "1." In the particular conditions of the experiments described below the distance from the magnetron etching zone to the substrate center was ~42 mm, since the main flow of atoms arrived onto the substrate surface at an angle of ~45 deg. The mean-free path for atoms in Ar atmosphere takes the same value for an argon pressure of ~1.3 mTorr. Therefore to manipulate the energy of deposited particles, we fabricated a series of ML samples with a sequential change in Ar pressure ranging from 1 to 4 mTorr. The mean-free path in doing so varied from ~53 mm down to ~13 mm, respectively.

Since interlayers in Mo/Si MXMs are silicides, the formation of each interlayer is accompanied by volume contraction because the total volume of the parent components involved in the reaction is larger than the volume of the reacted products. Maximal contraction is expected when $MoSi_2$ is formed, and for tabulated densities it reaches up to ~27.2%. This contraction should decrease the MXM periodicity compared to the expectation. We exploited this fact in evaluating the degree of layer interaction. Thus, we took the

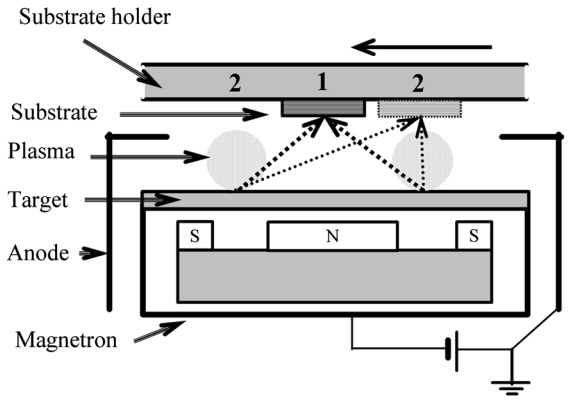

Fig. 1 A schematic view of a magnetron unit illustrating sputter/deposition geometry. The numeral "1" denotes a substrate position where major portion of each layer is deposited. Numerals "2" denote positions over the erosion zone, in which the substrate passes coming up to or going out from the magnetron. The arrow on the top shows the direction of substrate movement. The dotted arrows show the travel direction of sputtered particles from the magnetron target to the substrate.

difference, Δd, between expected MXM period, d_E, and experimental one, d_M, as a measure of intermixing and interaction in the Mo–Si ML system.

If the deposition rates and times are known, the values of the expected periods (d_E) can be estimated by the following formula:

$$d_E = V_{Mo} \times \tau_{Mo} + V_{Si} \times \tau_{Si}, \quad (1)$$

where V_{Mo} and V_{Si} are the deposition rates of molybdenum and silicon layers, respectively; and τ_{Mo} and τ_{Si} are the deposition times of Mo and Si layers, respectively.

In order to measure the real deposition rates of components, we followed the method described earlier.[65] To do this, we fabricated MXMs consisting of three periodic stacks differing by the deposition time of each component. In two sequentially deposited stacks, we changed the deposition time for only one component while the time for the other was the same. The difference in periods for adjacent stacks divided by the difference in times gave the deposition rate of the given component. The period of each deposited stack was determined on the base of the full Bragg equation adjusted for refraction, employing a least-squares method.

It should also be noted that two ML samples were fabricated in each experiment (labeled *A* and *B*), which were fixed on the rotating substrate holder on diametrically opposite sides. This was made to improve the reliability of the findings. The layered construction of *A* and *B* samples is asymmetric relative to each other in the sense that increasing deposition time for one of the component (e.g., for Mo) at the sample *A* is automatically attended by increasing deposition time for another component (i.e., Si) at the sample *B*. Thus, two of three stacks in the sample *A* contain thinner Mo layers while there are two stacks of thicker Mo layers in the sample *B*, and vice versa that occurs for Si layers.

3.2 *Small-angle Measurements at Hard X-rays ($\lambda = 0.154$ nm)*

Results on measuring deposition rates for Mo and Si in the range of sputtering pressures of 1 to 4 mTorr are presented in Fig. 2. As can be seen, the rates for corresponding components of the *A* and *B* series are close. The small variations are mainly connected with a slight difference in geometrical arrangement during the process of the deposition (magnetron-substrate distance, discharge parameters, etc.) in *A* and *B* positions. Generally, deposition rates for both series progressively decrease as the pressure increases, which is related to the decaying glow-discharge potential for each magnetron. The exception is the region of large pressures: at ~3 mTorr, a growth of deposition rates is observed. This was unexpected since it is not consistent with the data on the sputtering parameters. It is known that the deposition rate of sputtered matter varies directly with the electric power consumed by a magnetron.[66] However, we observe only a decay of the power for each magnetron when the Ar pressure increases. Thus, the apparent "increase" of deposition rates is a property of the sputtered ML rather than a result of changing the parameters of the magnetron glow discharge. We will return to possible explanations for this effect later.

Now knowing all constituents in Eq. (1), we determine the expected values of periods (d_E) and find the difference (Δd) between expected and measured (d_M) periods, i.e., the ML contraction. We attribute the differences directly to the interlayer interaction in Mo–Si system now and consider other possible reasons for contraction later. Processed data for all experiments are combined in Fig. 3. As illustrated, the contraction with the pressure does not vary monotonically: at low pressures (1.0 to 1.6 mTorr) it is relatively unaffected (0.36 to 0.49 nm) and then drops sharply at least by a factor of 5 down to 0.02 to 0.08 nm at 2.0 to 2.6 mTorr. Such a decrease in Δd suggests a noticeable decline in intermixing in the Mo–Si ML system. The pressure at which the decrease begins is ~1.8 mTorr, and the contraction approaches its minimum at ~2 mTorr. At this pressure, the mean-free path is comparable to the distance between the magnetron and the substrate. At 3 mTorr and above the contractions increase markedly again, and their values eventually exceed those for low pressures ($p < 1.6$ mTorr). This effect is observed for the same pressures as the deviation in deposition rates (see Fig. 2).

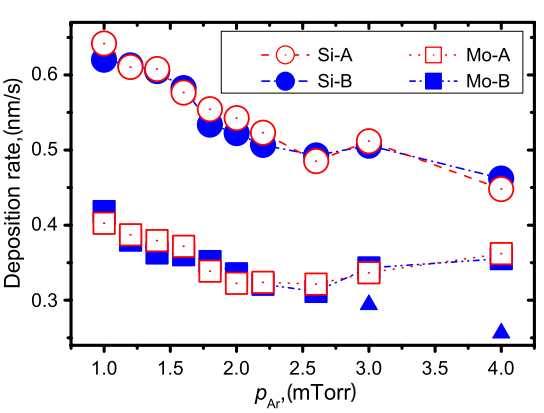

Fig. 2 Dependences of Mo and Si deposition rates (squares and circles) for Mo/Si ML series of A and B versus Ar working gas pressure. Triangles designate deposition rates for Mo extrapolated from the low pressure rates ($p < 2.6$ mTorr) with regard to direct proportionality of the deposition rate and the electric power consumed by the Mo-magnetron.

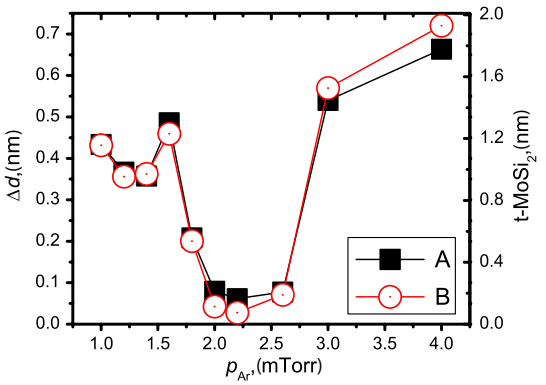

Fig. 3 The dependence of period contraction (left axis) and total disilicide interlayer thickness (right axis) for Mo/Si MLs versus Ar pressure.

We surmise that the contraction growth at $p \geq 3$ mTorr arises as follows. Molybdenum in Mo/Si multilayered samples can be in two states: crystalline or amorphous.[53] Although the transition from amorphous to crystalline states itself occurs sharply (within ~0.2 nm[38]), it is observed in the range of thicknesses $t_{Mo} \sim 2.0$ to 2.6 nm given by different authors.[38,43] Total thicknesses of silicide interfaces in Mo layers differs by 0.3 to 0.7 nm for these states. Thus, the amorphization of Mo layers produces an increase in period contraction. Evaluated by the measured deposition rates the thickness of the thinnest Mo layers in our samples for Ar pressures of 3 and 4 mTorr is 2.8 to 2.9 nm, that is outside the limits of the amorphous-crystalline transition. However, we also made an estimate of Mo deposition rates assuming that they varied directly with the applied power and found that the real thickness could be less, taking values of 2.1 to 2.4 nm (triangles in Fig. 2), that are within the amorphization range. Since each sample has ML stacks with two distinct thicknesses of molybdenum, the visible growth of Mo deposition rates must be connected with the difference in the structural states of thin and relatively thick Mo layers at the boundary of the amorphous-crystal transition. In this case, the effect of contraction decrease can be distorted.

As stated above, $MoSi_2$ is considered to be the main silicide formed at interfaces during sputter deposition.[35,38,49,50,52] With a formal approach to the description of the disilicide reaction ($Mo + Si \rightarrow MoSi_2$) and tabulated densities of components ($\rho_{Si} = 2.332$ g/cm^3, $\rho_{Mo} = 10.218$ g/cm^3, $\rho_{MoSi_2} = 6.24$ g/cm^3), we calculated volume ratios of components and the expected contraction (ΔV). A desired relation is $V_{MoSi_2}/\Delta V = 2.68$. Assuming that the reaction of silicide formation takes place normally to interfaces, this relation can be rewritten as $t_{MoSi_2} = 2.68 \times \Delta d$. Because the coefficient connecting the contraction and disilicide thickness changes only the scale of the pressure dependence, we just added one more axis in Fig. 3 (on the right) attributed to the thickness of formed disilicide.

Interlayer thicknesses obtained in this study (Fig. 3) are slightly thinner than literature values usually taken by the TEM method. On the one hand, small tilt of the samples in the TEM column and interfacial roughness may be responsible for larger values of the interface thickness. On the other hand, the density of formed silicide can be different from the tabulated one that is observed for thin films,[67,68] therefore actual silicide thickness may be larger.

At low pressures (<1.8 mTorr), where sputtered atoms do not strike neutral Ar atoms on the way to the substrate, the deposition of Mo atoms onto the substrate moving directly over the erosion zone (position 2 on the right of Fig. 1) may give rise to intermixing. According to TRIM-2008,[69] at a normal incidence the Mo atoms can penetrate deeper into *a*-Si and silicide subsurfaces, namely, ~1.3 and ~0.8 nm, respectively. These values are twice as large as the respective penetrations for the substrate located over the magnetron center (position 1 in Fig. 1) where Mo atoms are deposited at angles of ~45 deg. The largest thickness of the Mo layer deposited on the way to the magnetron is estimated to be ~0.08 nm and depends on the Ar pressure. Such a preliminary deposited Mo layer together with 0.17 to 0.20 nm deposited directly over the erosion zone (position 2 on the right of Fig. 1) may bring about the formation of a disilicide layer ~0.7-nm thick to a depth of ~1 nm. Interaction of molybdenum deposited over the magnetron center with an Si layer (position 1 in Fig. 1) completes the creation of the intermixed zones at low Ar pressures. Although the effective thickness of the Mo layer deposited on the moving substrate decreases with Ar pressure as Mo deposition rate also decreases, that cannot be the main reason for the drastic period contraction at ~2 mTorr, since the reductions of the Mo layer thickness and the corresponding silicide interlayer thickness should be at most ~0.1 and ~0.3 nm, respectively, for the whole studied pressure range. That is, considerably less than the observed decrease of the interlayer thickness (at least 0.8 nm, see Fig. 3, right axis).

Therefore, experimental evidence and rough estimation suggest that a considerable part of the silicide zone may be formed as the substrate moves around and the Mo atoms striking the substrate surface normally (position 2 in Fig. 1) make the main contribution.

3.3 *X-ray Fluorescent Analysis*

To make sure that our previous arguments concerning deposition rates were reasonable, we measured the intensities of the Mo Kα line in the samples of the *A* series with the x-ray wavelength dispersive spectrometer (SPRUT). The line was excited with an x-ray tube with an Ag anode. For calibration purposes, we used an etalon line of Br Kα from a thin fiberglass plastic plate used as a window and a sample stage simultaneously. All the measured data were divided by the corresponding Br Kα intensity taken in each measuring run and normalized by the maximal value. The results are shown in Fig. 4. We can see that for the whole range of Ar pressures the signal intensity only decreases. Though the given intensities are not a direct measure of the Mo atom quantity of the corresponding sample, the general tendency of the deposition rate decaying is still clearly visible.

3.4 *Phase Composition of Mo/Si MXMs*

Since the nonmonotonic decay of the deposition rate with an increase in Ar pressure may be associated with the amorphous-crystalline transition for Mo layers, we also analyzed the structural state of the Mo in all the samples. The examination of large-angle diffraction curves revealed that the Mo layers are crystalline (Fig. 5). Any reflections corresponding to silicon or silicide interlayers, that suggest their crystalline structure with the exception of a wide halo at $2\theta \sim 28$ deg, are absent. Diffraction patterns for samples of *A* and *B* series

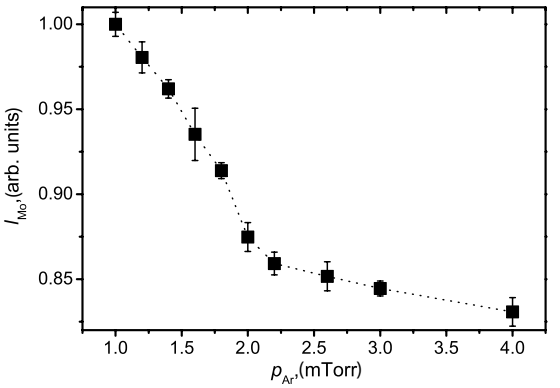

Fig. 4 Intensities of Mo Kα fluorescent line for Mo/Si ML samples deposited at different Ar pressures.

except for those made at 4 mTorr are almost identical to each other. That is a fair indication that at least within the pressure range of 1.0 to 2.6 mTorr where the pronounced drop in the contraction is observed (Fig. 3), there are no changes in the structural state of Mo layers.

Also present in the diffraction patterns is a sequential shift in the position of bcc Mo(1 1 0) peaks from $2\theta \sim 40.5$ deg (1 mTorr) to ~40.2 deg (4 mTorr), i.e., interplanar spacings for Mo(1 1 0) grow with pressure. Thick molybdenum single layers ($t_{Mo} > 50$ nm) deposited by magnetron sputtering at low Ar pressures (≤1 mTorr) are described[70] to have compressive stress. When the pressure increases, the transition from compressive to tensile stresses occurs around 2 mTorr. Such transition must be accompanied by decreasing the interplanar spacing for the atomic planes being parallel or at a small angle to the film plane at the expense of a lateral contraction. All that should be followed by the corresponding shift of diffraction peaks to larger angles. We have also made a measurement of stresses in Mo layers of ML samples by the $\sin^2 \Psi$ method to reveal that for the full range of Ar pressures Mo crystallites are under tensile stress with little change of the stress rate near 0.5 MPa. As we can see the opposite situation occurs in the diffraction patterns. So, the observed shift of peak position is not associated with stresses.

In our earlier study on MXMs with *a*-Mo ($t_{Mo} < 2$ nm) we found that the angular position of the most intense peak, associated with Mo, shifted from $2\theta \sim 43$ deg down to $2\theta \sim 40$ deg when Mo thickness grew from ~0.3 up to ~2 nm. Assuming that up to $t_{Mo} \sim 0.6$ nm Mo is in a bound state and after that a layer of *a*-Mo should appear, we subtracted the 0.9-nm Mo diffraction curve from that with $t_{Mo} \sim 1.9$ nm to get a diffraction curve characteristic for the pure amorphous molybdenum layers. The derived peak was located at $2\theta \sim 39.9$ deg while the tabulated position of Mo(1 1 0) must be at 40.49 deg with CuKα radiation. Therefore, we believe that the observed displacement of the angle position for Mo(1 1 0) by ~0.3 deg with an increasing pressure implies a tendency toward amorphization of Mo layers deposited at elevated pressures ($p \geq 3$ mTorr).

In addition to this finding a noticeable deterioration of the structural perfection of Mo crystals occurs at 4 mTorr: the full width at half maximum of Mo(1 1 0) is almost doubled, a noticeable decrease of its intensity compared to that for the 1-mTorr sample, a disproportionate lowering of intensities for other diffraction peaks (Fig. 5). For the samples of the *A* and *B* series with predominantly thin and thick Mo layers, respectively, the intensities of the Mo(1 1 0) peaks differ by a factor of ~2. All these data point to the possibility of existing *a*-Mo in thin layers of the samples deposited at 3 and 4 mTorr.

Thus, the amorphization of thin Mo films may bring about the overestimation of deposition rates for components at the boundary of the amorphous-crystalline transition for Mo layers deposited at Ar pressures of $p \geq 3$ mTorr.

3.5 *Transmission Electron Microscopy Study*

Separately for cross sectional TEM study, we prepared ML samples on silicon wafers at Ar pressures of 1.4, 2, and 4 mTorr and their periods were 15 to 16 nm. Such relatively large periods were chosen to avoid an appearance of *a*-Mo layers and to study MXMs with c-Mo layers only. In addition, in such samples the intermixed interlayers between amorphous silicon and crystalline molybdenum layers are easily revealed.

In cross sectional TEM images (Figs. 6 and 7) the crystalline grains are observed within the Mo containing layers at the expense of diffraction contrast. The grains are single block and their height conforms to the *c*-Mo layer thickness. Their dimensions sideward are many times longer and reach ~30 nm. According to the selected area electron diffraction patterns (not shown) the Mo-grains are textured for all samples. The texture axis [1 1 0] is perpendicular to the layers. Silicon layers are amorphous and separated from *c*-Mo layers by amorphous interlayers. They are well revealed owing to a phase contrast appearing when the objective lens is slightly defocused (~20 nm).

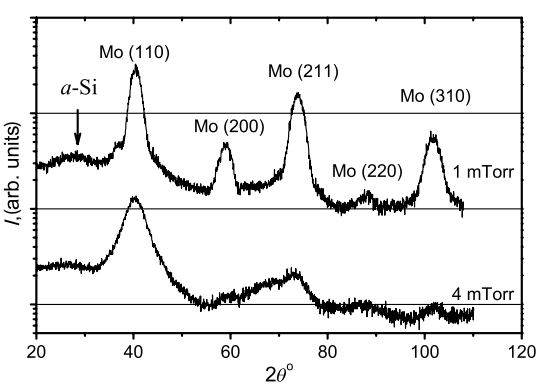

Fig. 5 Large-angle diffraction curves for Mo/Si MXMs demonstrating changes in Mo layer structure as a function of working gas pressure. Curves are shifted apart for convenience.

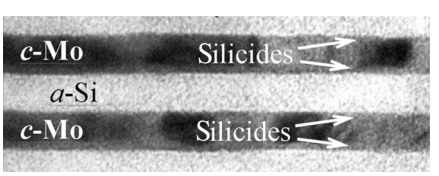

Fig. 6 Cross-sectional TEM image of Mo/Si multilayer x-ray mirror (MXM) deposited at 1.4 mTorr. The ML period is ~14.8 nm. The substrate is below.

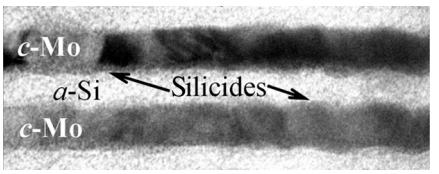

Fig. 7 Cross-sectional TEM image of Mo/Si MXM deposited at 4 mTorr. The ML period is ~16.4 nm. The substrate is below.

An interlayer width at Mo-on-Si interfaces for the sample deposited at 1.4 mTorr (Fig. 6) is 1.2 to 1.4 nm. At adjacent interfaces (Si-on-Mo ones) the interlayers are thinner: 0.7 to 0.8 nm. The rise of the Ar pressure to 2 mTorr does not involve any substantial changes in the structure. A 0.2-nm reduction of the interlayer widths was noted but this value is comparable with the microscope resolution. Slight increase of the interface roughness could be seen at this pressure. Further growth of the pressure until 4 mTorr (Fig. 7) is accompanied by an appreciable development of the interface roughness rising from the substrate to the surface and a deterioration of the axial texture perfection. Meanwhile, the visible thickness of interlayers at the bottom Mo interface decreases down to ~1 nm.

Figure 8 shows typical values of total silicide thickness (circles) of adjacent interlayers taken from TEM cross-sections. Interlayer thicknesses (squares) derived from small-angle x-ray measurements (Sec. 3.2) assuming their disilicide character are also added for comparison. As one can observe in Fig. 8, there is virtually no correlation between TEM and x-ray data. In general, they differ considerably, especially within the pressure range of 2 to 2.6 mTorr where the difference may approach 1 order of magnitude. The measurements of interlayer widths agree only for samples deposited at the Ar pressure of 3 mTorr and above. Although TEM measurements may give overestimates, the discrepancy is apparent and, on the whole, x-ray data are inferior to TEM data.

3.6 *Probe Potential Measurement*

Since the substrate is close to the magnetrons, a potential can be induced on its surface when subjected to the magnetron plasma. This can interfere with the interlayer formation process. So, we made a probe measurement of the potential with a cylinder Langmuir probe. The probe comprises a tungsten wire ~0.2-mm thick placed within a ceramic tube.

We did not find any measurable potential over the magnetron centers (at ~30 mm) in the whole range of Ar pressures. However, some plasma glow far from the target visible through the vacuum chamber window in the absence of the substrate necessitated more detailed probe measurements over the whole magnetron surface.

Figure 9 shows results of such a probe test over the Si and Mo targets at $p_{Ar} = 1.2$ mTorr. It is seen that within the magnetron center ($-20 < r < 20$ mm) of both magnetrons a floating potential is negligible. This area corresponds to the substrate position where the major portion of the matter is deposited (position 1 in Fig. 1). Here, we can also see that outside the central region the variation of the floating potential is more pronounced. For example, for Si (circles in Fig. 9) it varies from 0 down to −13.8 V in the region denoted by the numerals "2" (Fig. 1). Peak positions make it possible to determine the diameter of plasma rings, ~77 mm for Si and ~72.5 mm for Mo. The shapes of the potential curves for Mo and Si magnetrons are similar but on a reduced scale for Mo (around a third). We also investigated the sputtered targets directly. The width of sputtered zones is ~1 cm. Erosion is nonuniform within the zone, and the diameter of the deepest part is ~67 mm. We inserted these measurements in Fig. 9 represented schematically at the bottom of the figure as a gray target section. The diameters of the plasma rings are larger than the erosion zones by ~10 mm for Si and ~5.5 mm for Mo targets, i.e., broadening of plasma rings is observed over both targets. This phenomenon is associated with an asymmetry of magnetic lines from the magnetron magnetic poles implying an expansion of the plasma rings in the area of probe measurements.

These pronounced potentials vary with the Ar pressure. Their variations are presented in Fig. 10 for the positions of maximal potential values of each magnetrons. For the Si magnetron, the floating potential drops from −17 to −13 V over the pressures of 1 to 1.3 mTorr and then actually it does not change. For the Mo magnetron, the variation is more complex: the floating potential grows from −2.5 up to −4.2 V (1 to 1.2 mTorr), then drops down to −2V (1.3 to 2.2 mTorr) and then gradually recedes almost to 0.

The observed maximum potentials are less than the sputter threshold energies for both components ($E_{th}^{Si} \sim 43.2$ and $E_{th}^{Mo} \sim 38.7$ eV/atom according to Ref. 71) even if we use rough estimates of the requisite energies expressed as $E_{th} \sim 4E_B$ (18.7 and 27.5 eV/atom for Si and Mo, respectively[72]).

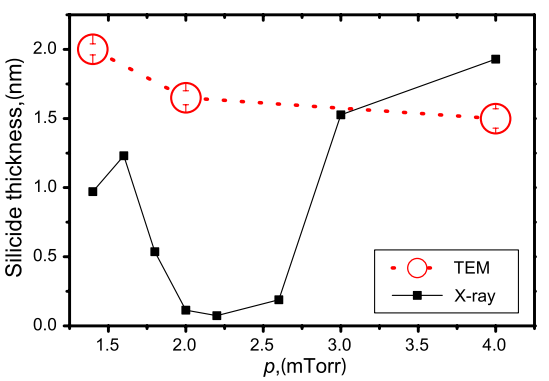

Fig. 8 Interlayer silicide thickness (circles) taken by cross-sectional TEM method versus Ar pressure. X-ray data (squares) estimated on the assumption of disilicide character of interlayers are added for comparison.

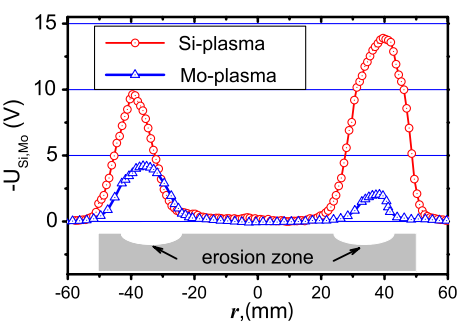

Fig. 9 Results of probe measurements over the silicon (circles) and the molybdenum (triangles) magnetrons at Ar pressure of 1.2 mTorr.

So we cannot expect any re-sputtering of Si and Mo layers during the deposition process from this effect.

It is also known that a deposited film can be re-sputtered by the noble gas neutrals reflected from the target.[73] However, the magnetron potentials are practically unaffected by the Ar pressure (changes <6%) with no noticeable features in the range of 1.4 to 2 mTorr.

The shortest distance between the erosion zone and the substrate is ~30 mm, which corresponds to the mean-free path at an Ar pressure of ~1.75 mTorr, i.e., the pressure of drastic decrease in the contraction (Fig. 3). Tangible decrease of floating potential begins at 1.1 mTorr for Si and at 1.4 mTorr for Mo (Fig. 10), i.e., at pressures appreciably <2 mTorr. Thus, the impact of the floating potential at the substrate on the interlayer formation is negligible.

These considerations suggest that the magnetron plasma has a little effect on the ML contraction at ~2 mTorr (Fig. 3). So, it again justifies the use of the volume contraction (see Sec. 3.2) as a measure of interface intermixing in the Mo–Si ML system.

3.7 *Extreme Ultraviolet Measurements*

We measured the EUV reflectivity of single period Mo/Si MXMs ($d \sim 7$ nm) prepared at Ar pressures ranging from 1.4 up to 2.6 mTorr. That pressure range includes the critical point (~2 mTorr) with the key feature in the period contraction (Sec. 3.2). MXM characteristics and results of measurements are tabulated in Table 1 and depicted in Fig. 11. It is seen from the table that reflectivities in the hard x-ray and EUV ranges are not correlated.

The pressure dependence of the EUV reflectivity is a nonmonotonic function (Fig. 11). There is a maximum around 2.2 mTorr. Reflectivity growth at low pressures ($1.4 < p < 2.2$ mTorr) implies that the refractive index gradient at the Mo–Si interfaces increases, i.e., the degree of silicide formation at the interfaces diminishes. Above 2.4 mTorr, the reflectivity goes down. Such reduction must be concerned with the development of interface roughness at higher pressure. This is demonstrated in the TEM results of this study (see Sec. 3.5) and in studies of other authors.[57,74] The existence of a maximum reflectivity demonstrates that there is a trade-off between rise of optical contrast and roughness development.

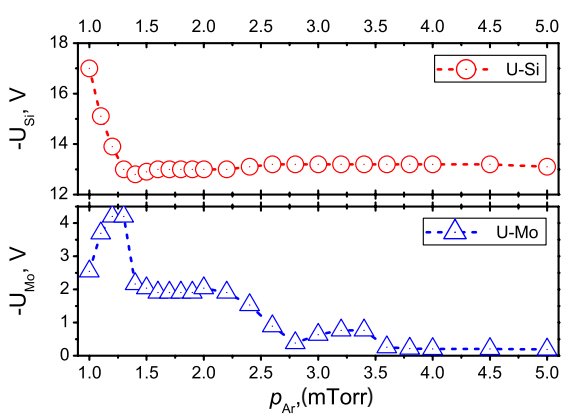

Fig. 10 Maximal floating potentials measured with the probe separated from Si and Mo magnetron surfaces by the distance of ~30 mm.

Table 1 Parameters of Mo/Si multilayer x-ray mirrors and results of measuring the reflectivities in EUV ranges at near normal incidence ($\theta = 85$ deg).

No.	p_{Ar} (mTorr)	d (nm)	R_1 (%) (0.154 nm)	R (%) (normal incidence)	λ (nm)	$\Delta\lambda$ (nm)
1	1.4	6.87	73.6	54.6	13.4	0.51
2	1.8	6.91	72.0	59.9	13.4	0.51
3	2.0	6.95	72.6	61.3	13.5	0.52
4	2.6	6.84	71.1	59.9	13.3	0.49

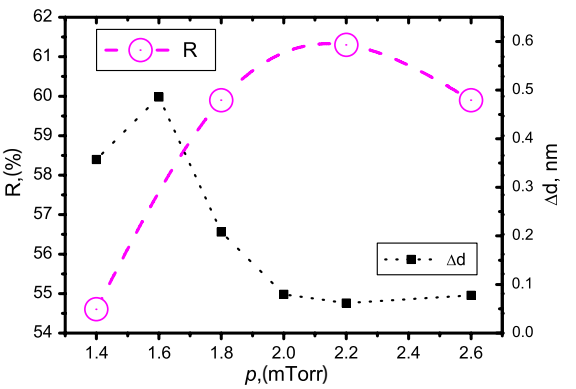

Fig. 11 Extreme ultraviolet ($\lambda = 13.2$ to 13.6 nm) normal incident reflectivity of Mo/Si MXMs versus the Ar pressure. The dependence of ML period contraction is added for convenience. Connecting lines are just guides for the eyes.

4 Discussion

As was shown in Sec. 3.5, there is a weak tendency for the interlayer thickness to decrease as the pressure grows, in spite of the fact that the estimated contractions demonstrate their significant reduction (see Sec. 3.2). The total thickness of the $MoSi_2$ interlayers, according to our estimates, is no more than 0.21 nm at intermediate pressures ($1.8 < p < 3.0$ mTorr). At the same time, the interlayers for Mo-on-Si interfaces in the TEM images are at least 1-nm thick, i.e., about five times larger. One possible explanation of this contradiction is a modification of the interface composition with the pressure variation.

There are experimental data for e-beam MLs demonstrating formation of interlayers with a composition of Mo-enriched silicides,[75] e.g., Mo_5Si_3[39,55] and Mo_3Si.[55] It was also shown that the interlayer composition is changed from Mo_5Si_3 to $MoSi_2$ depending on the energy of Kr^+ ions used for smoothing Si layer surfaces.[40] The energy of atoms deposited from the thermal sources is low (0.1 to 0.2 eV). Thus, the formation of lower silicides could be expected for such deposition methods. However, it was shown by Maury et al.[76] that in sputter-deposited Mo/Si MXM (the energy of Mo atoms is at least one order of magnitude higher compared to that for thermal evaporation), the Mo_5Si_3 silicide is formed at Mo-on-Si interfaces. From the data reported in the literature, it is possible to discern for

Si-enriched silicides to appear as the energy released at interfaces increases. This is also confirmed in growing of amorphous interlayers with a composition of $MoSi_x$ ($x \sim 3.9$) in the presence of irradiating Mo/Si MXMs with Ar^+ ions having the energy of ~180 keV.[77]

Having made the estimations of Sec. 3.2, we found that volume ratios between a silicide and the corresponding contraction came to $V_{Mo5Si_3}/\Delta V \sim 4.8$ for Mo_5Si_3 ($\rho_{Mo_5Si_3} = 8.24$ g/cm^3) and to $V_{Mo_3Si}/\Delta V \sim 7.1$ for Mo_3Si ($\rho_{Mo_3Si} = 8.97$ g/cm^3). Then minimal contraction of 0.07 to 0.21 nm (Fig. 3) must give rise to Mo_5Si_3 0.34- to 1.01-nm thick or Mo_3Si 0.5- to 1.49-nm thick. We correlated our estimations with the TEM data (Sec. 3.4) and concluded that one of the interfaces in Mo/Si MXMs deposited at Ar pressures $p \geq 2$ mTorr has a composition close to Mo_5Si_3 or silicide mixture of Mo_5Si_3 and Mo_3Si.

It should be noted that in an MXM performance simulation the replacement of one silicide by another in the interlayer composition increases the estimated ML reflectivity by ~2.7% only against experimentally observed 6.7%, even if we take marginal silicides (i.e., $MoSi_2$ and Mo_3Si). Now, we have no appropriate explanation for this fact, although some attendant processes may double the estimated value, among which are thinning the silicide interlayers, lowering Ar content in Si layers, reducing the number of dissolved Si atoms in c-Mo layers, etc.

5 Conclusions

It is experimentally shown that a reduction in the period contraction and amorphous interlayer thickness in Mo/Si MXMs deposited by the magnetron sputtering is observed when Ar pressure increases from 1 to 4 mTorr. The critical pressure giving the maximal drop in the period contraction (~2 mTorr) correlates with the pressure at which the mean-free path for the atoms in the Ar working gas is comparable with the shortest distance between the magnetron and the substrate. The contraction is a result of a change in the interlayer composition from $MoSi_2$ to Mo_5Si_3 or the mixture of Mo_5Si_3 and Mo_3Si. The composition change and thinning of the interlayer thickness is connected with the decreasing energy of atoms deposited onto the growing surface at the expense of collisions with working gas atoms and a transfer to them of an excessive energy.

The interlayer composition changeover is attended by the growth of Mo/Si MXM reflectivity in the EUV region by 6.7%.

A new study is now in progress to optimize the construction of Mo/Si MXMs and the deposition technology.

Acknowledgments

Y. P. P. is acknowledged to ISKCON for improving the realization with regard to the place of this work. This work was supported by the US Department of Energy under contract number DE-AC02-05CH11231.

References

1. A. M. Khounsary, C. Morawe, and S. Goto, Eds., *Proc. SPIE* **6705** (2007).
2. A. M. Khounsary, C. Morawe, and S. Goto, Eds., *Proc. SPIE* **7077** (2008).
3. A. M. Khounsary, C. Morawe, and S. Goto, Eds., *Proc. SPIE* **7448** (2010).
4. C. Morawe, A. M. Khounsary, and S. Goto, Eds., *Proc. SPIE* **8139** (2011).
5. L. Assoufid, P. Z. Takacs, and A. K. Asundi, Eds., *Proc. SPIE* **8501** (2012).
6. C. W. Gwyn et al., "Extreme ultraviolet lithography," *J. Vac. Sci. Technol. B* **16**(6), 3142–3149 (1998).
7. R. H. Stulen and D. W. Sweeney, "Extreme ultraviolet lithography," *IEEE J. Quant. Electron.* **35**(5), 694–699 (1999).
8. J. Benschop et al., "Extreme ultraviolet lithography: status and prospects," *J. Vac. Sci. Technol. B* **26**(6), 2204–2207 (2008).
9. V. Bakshi, Ed., *EUV Lithography*, p. 673, SPIE Press, Bellingham, WA (2009).
10. I. A. Artyukov et al., "Soft X-ray submicron imaging experiments with nanosecond exposure," *Opt. Commun.* **102**(5–6), 401–406 (1993).
11. F. Brizuela et al., "Microscopy of extreme ultraviolet lithography masks with 13.2 nm tabletop laser illumination," *Opt. Lett.* **34**(3), 271–273 (2009).
12. L. Golub et al., "Sub-arcsecond observations of the solar X-ray corona," *Nature* **344**(6269), 842–844 (1990).
13. L. Golub et al., "A photometric imaging solar telescope, tunable in the extreme ultraviolet, utilizing multilayer X-ray optics," *Rev. Sci. Instrum.* **73**(4), 1908–1913 (2002).
14. V. E. Levashov et al., "High throughput and resolution compact spectrograph for the 124–250 Å range based on $MoSi_2$–Si sliced multilayer grating," *Opt. Commun.* **109**(1–2), 1–4 (1994).
15. H. Blaschke et al., "Optics characterization with compact EUV spectrophotometer," *Proc. SPIE* **6922**, 692228 (2008).
16. L. B. Da Silva et al., "Extreme-ultraviolet interferometry at 15.5 nm using multilayer optics," *Appl. Opt.* **34**(28), 6389–6392 (1995).
17. F. Delmotte et al., "X-ray-ultraviolet beam splitters for the Michelson interferometer," *Appl. Opt.* **41**(28), 5905–2912 (2002).
18. S. de Rossi et al., "Probing multilayer stack reflectors by low coherence interferometry in extreme ultraviolet," *Appl. Opt.* **47**(12), 2109–2115 (2008).
19. W. Hu et al., "Transmission multilayer polarizers for use in the 55–90 eV region," *J. Synchrotron Radiat.* **5**(3), 732–734 (1998).
20. Z. Wang et al., "Broadband multilayer polarizers for the extreme ultraviolet," *J. Appl. Phys.* **99**(5), 056108 (2006).
21. E. A. Vishnyakov et al., "Aperiodic multilayer structures in soft X-ray radiation optics," *Quant. Electron.* **42**(2), 143–152 (2012).
22. S.-I. Han et al., "Design and method of fabricating phase-shift masks for extreme-ultraviolet lithography by partial etching into the EUV multilayer mirror," *Proc. SPIE* **5037**, 314–330 (2003).
23. Z. Wang et al., "Broadband Mo/Si multilayer transmission phase retarders for the extreme ultraviolet," *Appl. Phys. Lett.* **90**(3), 031901 (2007).
24. H. Y. Kang and C. K. Hwangbo, "Optical design of hybrid-type attenuated phase-shift masks for extreme-ultraviolet lithography by use of a Fabry–Perot interference filter," *Appl. Opt.* **47**(13), C75–C78 (2008).
25. T. Haga et al., "Soft X-ray multilayer beam splitters," *J. Synchrotron Radiat.* **5**(3), 690–692 (1998).
26. H. Takenaka et al., "Fabrication of soft X-ray beam splitters for use in the wavelength region around 13 nm," *J. Phys. IV* **104**, 251–254 (2003).
27. H. Takenaka, S. Ichimaru, and E. M. Gullikson, "Development of beam splitters for EUV region," in *Proc. 8th Int. Conf. X-ray Microscopy, IPAP Conf. Series*, Vol. 7, pp. 198–200 (2006).
28. A. L. Aquila et al., "Developments in realistic design for aperiodic Mo/Si multilayer mirrors," *Opt. Exp.* **14**(21), 10073–10078 (2006).
29. A. G. Michette and Z. Wang, "Optimisation of depth-graded multilayer coatings for broadband reflectivity in the soft X-ray and EUV regions," *Opt. Commun.* **177**(1–6), 47–55 (2000).
30. M. Schultze et al., "Powerful 170-attosecond XUV pulses generated with few-cycle laser pulses and broadband multilayer optics," *New J. Phys.* **9**(7), 243 (2007).
31. N. P. Lyakishev and O. A. Bannyh, Eds., *Handbook on Binary State Diagrams of Metallic Systems*, p. 448, Mashinostroenie, Moscow (2000) (in Russian).
32. A. K. Petford-Long et al., "High-resolution electron microscopy study of X-ray multilayer structures," *J. Appl. Phys.* **61**(4), 1422–1428 (1987).
33. M. B. Stearns, C.-H. Chang, and D. G. Stearns, "Optimization of growth conditions of vapor deposited Mo/Si multilayers," *J. Appl. Phys.* **71**(1), 187–195 (1992).
34. C. Largeron, E. Quesnel, and J. Thibault, "Interface growth mechanism in ion beam sputtering-deposited Mo/Si multilayers," *Philos. Mag.* **86**(19), 2865–2879 (2006).
35. P. Boher et al., "Structural characteristics and performances of rf-sputtered Mo/Si and Co/Si multilayers for soft X-ray optics," *Proc. SPIE* **1547**, 21–38 (1991).
36. K. Hiruma et al., "Performance and quality analysis of Mo–Si multilayers deposited by ion beam sputtering and magnetron sputtering," *Proc. SPIE* **6151**, 61511V (2006).
37. S. Yulin et al., "Interlayer transition zones in Mo/Si superlattices," *J. Appl. Phys.* **92**(3), 1216–1220 (2002).
38. S. Bajt, D. G. Stearns, and P. A. Kearney, "Investigation of the amorphous-to-crystalline transition in Mo-Si multilayers," *J. Appl. Phys.* **90**(2), 1017–1025 (2001).

39. A. E. Yakshin et al., "Determination of the layered structure in Mo/Si multilayers by grazing incidence X-ray reflectometry," *Physica B* **283**(1–3), 143–148 (2000).
40. I. Nedelcu et al., "Interface roughness in Mo/Si multilayers," *Thin Solid Films* **515**(2), 434–438 (2006).
41. E. Louis et al., "Nanometer interface and materials control for multilayer EUV-optical applications," *Prog. Surf. Sci.* **86**(11–12), 255–294 (2011).
42. E. N. Zubarev et al., "Interface intermixed zones in Mo-Si multilayers," *Metallofiz. Noveishie Tehnol.* **19**(8), 56–63 (1997) (in Russian).
43. S. S. Andreev et al., "The microstructure and X-ray reflectivity of Mo/Si multilayers," *Thin Solid Films* **415**(1–2), 123–132 (2002).
44. K. Holloway, K. B. Do, and R. Sinclair, "Interfacial reactions on annealing molybdenum–silicon multilayers," *J. Appl. Phys.* **65**(2), 474–480 (1989).
45. D. G. Stearns et al., "Thermally induced structural modification of Mo–Si multilayers," *J. Appl. Phys.* **67**(5), 2415–2427 (1990).
46. D. L. Windt, R. Hull, and W. K. Waskiewicz, "Interface imperfections in metal/Si multilayers," *J. Appl. Phys.* **71**(6), 2675–2678 (1992).
47. L. Wu et al., "Interlayer microstructure of sputtered Mo/Si multilayers," *J. Phys.: Condens. Matter* **9**(17), 3521–3528 (1997).
48. W. L. Morgan and D. B. Boercker, "Simulating growth of Mo/Si multilayers," *Appl. Phys. Lett.* **59**(10), 1176–1178 (1991).
49. D. G. Stearns, R. S. Rosen, and S. P. Vernon, "High-performance multilayer mirrors for soft X-ray projection lithography," *Proc. SPIE* **1547**, 2–13 (1991).
50. S. Braun et al., "Mo/Si-multilayers for EUV applications prepared by pulsed laser deposition (PLD)," *Microelectron. Eng.* **57–58**, 9–15 (2001).
51. H. L. Meyerheim et al., "Amorphous molybdenum silicide layers and Mo/Si(100) interface growth: local structure and preparation dependence," *Phys. Rev. B* **41**(9), 5871–5880 (1990).
52. J. M. Slaughter et al., "Growth of molybdenum on silicon: structure and interface formation," *Phys. Rev. B* **44**(8), 3854–3863 (1991).
53. E. N. Zubarev et al., "Influence of the structural state for molybdenum layers on the formation of interlayer transition zones in Mo/Si multilayer compositions," *Metallofiz. Noveishie Tehnol.* **24**(10), 1429–1437 (2002) (in Russian).
54. R. M. Walser and R. W. Bené, "First phase nucleation in silicon-transition-metal planar interfaces," *Appl. Phys. Lett.* **28**(10), 624–625 (1976).
55. I. Nedelcu et al., "Temperature-dependent nanocrystal formation in Mo–Si multilayers," *Phys. Rev. B* **76**(10), 245404 (2007).
56. E. N. Zubarev et al., "The structure of Mo/Si multilayers prepared in the conditions of ionic assistance," *Appl. Phys. A* **90**(4), 705–710 (2008).
57. S. P. Vernon, D. G. Stearns, and R. S. Rosen, "Ion-assisted sputter deposition of molybdenum–silicon multilayers," *Appl. Opt.* **32**(34), 6969–6974 (1993).
58. A. Patelli et al., "Ion bombardment effects on nucleation of sputtered Mo nano-crystals in $Mo/B_4C/Si$ multilayers," *Surf. Coat. Technol.* **201**(1–2), 143–147 (2006).
59. A. F. Jankowski, "On eliminating deposition-induced amorphization of interfaces in refractory metal multilayer systems," *Thin Solid Films* **220**(1–2), 166–171 (1992).
60. T. Yamaguchi et al., "Reflective properties of Mo/Si multilayer for EUV lithography deposited by the magnetron sputtering device with superconducting bulk magnets," *Physica C* **468**(15–20), 2170–2173 (2008).
61. M. Niibe et al., "Fabrication of an aspherical mirror for extreme ultraviolet lithography (EUVL) optics," *Proc. SPIE* **3447**, 32–39 (1998).
62. N. Hosokawa et al., "Development of beam splitter using multilayer membrane for extreme ultraviolet phase-shift microscope," *Jpn. J. Appl. Phys.* **44**(7B), 5540–5543 (2005).
63. J. H. Underwood et al., "Calibration and standards beamline 6.3.2 at the advanced light source," *Rev. Sci. Instrum.* **67**(9), 3372 (1996).
64. E. Gullikson, http://cxro.lbl.gov/als632/ (2010).
65. C. Montcalm et al., "Extreme-ultraviolet Mo/Si multilayer mirrors deposited by radio-frequency-magnetron sputtering," *Appl. Opt.* **33**(10), 2057–2068 (1994).
66. V. E. Minaichev, V. V. Odinokov, and G. P. Tyufaev, "Magnetron sputtering equipment," *Rev. Electron. Eng.* **659**(8), 57 (1979) (in Russian).
67. A. F. Ruppert et al., "Density of ultrathin amorphous silicon and germanium sublayers in periodic amorphous multilayers," *Phys. Rev. B* **44**(20), 11381–11385 (1991).
68. J. Gautier et al., "Characterization and optimization of magnetron sputtered Sc/Si multilayers for extreme ultraviolet optics," *Appl. Phys. A* **88**(4), 719–725 (2007).
69. http://www.srim.org/.
70. D. W. Hoffman and J. A. Thornton, "Internal stresses in Cr, Mo, Ta and Pt films deposited by sputtering from a planar magnetron source," *J. Vac. Sci. Technol.* **20**(3), 355–358 (1982).
71. J. Bohdansky, J. Roth, and H. L. Bay, "An analytical formula and important parameters for low-energy ion sputtering," *J. Appl. Phys.* **51**(5), 2861–2865 (1980).
72. R. V. Stuart and G. K. Wehner, "Sputtering thresholds and displacement energies," *Phys. Rev. Lett.* **4**(8), 409–410 (1960).
73. M. M. Hasan, R. J. Highmore, and R. E. Somekh, "The uhv deposition of short-period multilayers for X-ray mirror applications," *Vacuum* **43**(1–2), 55–59 (1992).
74. M. Niibe et al., "Suppression of columnar-structure formation in Mo–Si layered synthetic microstructures," *Proc. SPIE* **1343**, 2–13 (1990).
75. B. Heidemann et al., "Interlayer composition and interface stability in Mo/Si multilayers studied with high-resolution RBS," *Appl. Surf. Sci.* **78**(2), 133–140 (1994).
76. H. Maury et al., "Non-destructive X-ray study of the interphases in Mo/Si and $Mo/B_4C/Si/B_4C$ multilayers," *Thin Solid Films* **514**(1–2), 278–286 (2006).
77. E. N. Zubarev et al., "Intermixing processes in Mo/Si multilayer periodic compositions irradiated by Ar^+ ions," *Metallofiz. Noveishie Tehnol.* **29**(12), 1555–1570 (2007) (in Russian).

Yuriy P. Pershyn graduated from Kharkiv Polytechnic Institute, USSR, in 1980. Since 1986, he has worked at the National Technical University "Kharkiv Polytechnic Institute." In 1991, he got his PhD degree with the thesis title: "Structure and thermal stability of Mo–Si based multilayers." He is an expert in fabrication and characterization of layered compositions. His fields of interest include structural and phase transformations in layers, multilayers during deposition, annealing and irradiation with x-rays, and formation of interfaces.

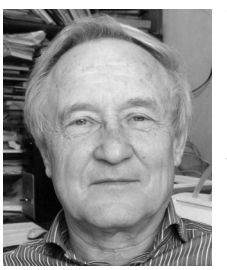

Valeriy V. Kondratenko graduated from Kharkiv Polytechnic Institute, USSR, in 1972. In 1999, he got his Doctor of Science degree with the thesis title: "Structural and phase transformation in nano-scale layered systems." Since 1972, he has worked at the National Technical University Kharkiv, Ukraine, in the field of thin film technology, superlattice and multilayer growth, x-ray optics and their applications. At present, he is the chief research scientist, professor. He has more than 150 scientific publications.

Valentine V. Mamon graduated from Kharkiv Polytechnic Institute in 1986. He participated in developing a crystal-diffractive instrument for nondestructive assay of materials and alloys. He is an expert in high-voltage portable power supplies for x-ray tubes and x-ray detectors.

Svetlana A. Reutskaya left her school with distinction in 2007 and went to the National Technical University, Kharkiv, Ukraine. Now, she is working on her degree in the topic "Formation of silicide interlayers in Mo/Si multilayers."

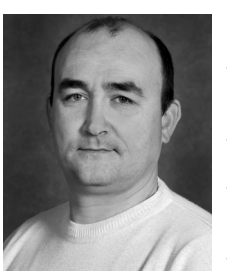

Dmitriy L. Voronov received his MS degree in physics of metals and semiconductors from Kharkiv Polytechnic Institute in 1989 and his PhD degree from Kharkov National University, Ukraine, in 2003. He has more than 40 scientific papers on development of multilayer mirrors, investigation of interdiffusion and phase transformation in multilayers, growth of multilayers on highly corrugates surfaces, and design, optimization, and characterization of diffraction gratings for x-rays. He currently works as a physicist project scientist

for Advanced Light Source, Lawrence Berkeley National Laboratory. His research activity is focused on development of highly efficient diffraction gratings for high spectral resolution EUV and soft x-ray applications.

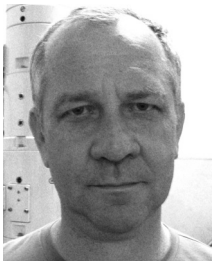

Evgeniy N. Zubarev graduated from the Kharkiv Polytechnic Institute (USSR) in 1981. Since 1981, he has worked at the Metal and Semiconductor Physics Department of the Kharkiv Polytechnic Institute (National Technical University from 2000). He is a doctor of science in physics and mathematics, with a specialty in solid state physics. He is an expert in high resolution transmission electron microscopy and x-ray diffractometry. His field of interests include structural and phase transformations in nanoscale multilayers during deposition, annealing and irradiation by accelerated particles, and x-ray laser radiation.

Igor A. Artyukov graduated from Moscow Engineering and Physics Institute, Russia, in 1988. In 1993, he got his PhD degree at Lebedev Physical Institute with the thesis title: "Optics for soft x-ray lithography and microscopy." Since 1991, he has worked at Lebedev Physical Institute in the field of x-ray optics and its applications. At present, he is the head research scientist. He has more than 70 scientific publications.

Alexander Vladimirovich Vinogradov is a professor. He graduated from Moscow Institute of Physics and Technology in 1964 and entered Lebedev Physical Institute as an engineer. His expertise is in the areas of atomic physics, x-ray optics, and x-ray lasers. In 1991 he was awarded with the State Prize in Physics and Technology for his work on x-ray optics, and in 2007 he won the Nikolai Basov Prize for "Development and Application of Reflective Optics for the wavelength range 35 to 60 nm."

Eric M. Gullikson: biography and photography is not available.